Journal of Structural Geology 132 (2020) 103975

Contents lists available at ScienceDirect

Journal of Structural Geology

journal homepage: http://www.elsevier.com/locate/jsg

Present day In-situ stress magnitude and orientation of horizontal stress components in the eastern Illizi basin, Algeria: A geomechanical modeling

Rafik Baouche [a], Souvik Sen [b,*], Khadidja Boutaleb [c]

[a] Department of Geophysic, Faculty of Hydrocarbons and Chemistry (FHC), University M'Hamed Bougara Boumerdes, 35000, Boumerdès, Algeria
[b] Geologix Limited, Dynasty Building, Wing A, Level 4, Andheri Kurla Road, Andheri (E), Mumbai, 400059, Maharashtra, India
[c] Department of Geology, Laboratory of Resources Minérals at Energétiques, Faculty of Sciences, M'Hamed Bougara University of Boumerdes, 35000, Boumerdès, Algeria

ARTICLE INFO

Keywords:
In-situ stress magnitude
Stress orientation
Pore pressure
Fault reactivation
Illizi basin

ABSTRACT

We analyzed drilling induced tensile fractures from resistivity image log data to ascertain the orientation of maximum horizontal stress (S_H) from the eastern Illizi basin, Algeria. An average S_H azimuth of 150°N (± 10°) has been interpreted from B-quality induced fractures, as per world stress map guidelines. The overall NW-SE orientation of S_H translates to the relative plate motion of the African and Eurasian plates. Vertical stress (S_v) gradient of 1.07 PSI/ft has been derived from density log. Pore pressure estimated from sonic slowness reveals overpressure in Silurian shale, deposited in a transgressive depositional environment, whereas Devonian and Ordovician hydrocarbon reservoirs have been seen to be normally pressured. Poroelastic strain model has been employed to quantify maximum and minimum horizontal stress (S_h) magnitudes. An effective stress ratio of 0.6, interpreted from leak-off test has also been used to model S_h. Using frictional faulting theory, upper limit of S_H has been quantified. S_H/S_v ratio of 1.04 (1.01–1.26) has been seen in the study area. Based on the relative stress magnitudes ($S_H > S_v > S_h$), a present day strike-slip faulting regime has been inferred in the eastern Illizi basin, Algeria. Fault reactivation potential at reservoir level has been inferred from stress polygon analysis.

1. Introduction

Reservoir geomechanical modeling has become an integral part of field development studies. It has critical implications in horizontal well placement, drilling and completion, reservoir development and abandonment (Sayers et al., 2002; Tingay et al., 2005, 2009; Meng et al., 2011; Ramdhan and Goulty, 2011; Hoesni, 2004). A comprehensive geomechanical model has five principal components: magnitude of three in-situ stresses, i.e. vertical stress (S_v), minimum horizontal stress (S_h), maximum horizontal stress (S_H); distribution of formation pore pressure (PP) and orientation of S_H (Tingay, 2015; Zoback, 2007; Rajabi et al., 2016). Accurate knowledge of pore pressure and in-situ stress distribution equips subsurface team to better plan well delivery and production optimization (Zhang, 2011, 2013; Sen et al., 2019, 2020).

In this study, we investigated an exploratory well, drilled in the Takouazet field, eastern Illizi basin, Algeria. Hydrocarbon discoveries have been established from the Devonian and Ordovician sandstone units. We took this opportunity to utilize the well data and perform a well-scale geomechanical modeling, being the first from this field. The primary objectives of this work are to estimate the magnitude of in-situ stress tensors and direction of S_H. A rock mechanical property based approach has been considered for this analysis that involves the available geophysical log data set as primary inputs and downhole measurements as calibration parameters. Based on the relative magnitudes of in-situ stress tensors, present day strike-slip faulting regime has been interpreted in the eastern Illizi basin. Drilling induced tensile fractures (DITF) have been interpreted from Formation micro-imager log (FMI) to decipher precise S_H azimuth and has been correlated with World Stress Map (WSM) database. Utilizing stress polygons, we analyzed the reactivation potential of critically oriented faults at Devonian and Ordovician reservoirs, and inferred the minimum pore pressure changes required during hydraulic fracturing to cause a fault slip.

2. Geological settings of the study area

The studied Takouazet field is situated at the eastern part of Illizi basin, In-Amenas area of southeast Algeria near to Algeria-Libya international border (Boote et al., 1998; Klett, 2000). Amguid-Hassi Touareg structural axis defines the western boundary, while Tihemboka Arch demarcates the eastern boundary. Hoggar massif and Ghadames

* Corresponding author.
E-mail address: souvikseniitb@gmail.com (S. Sen).

https://doi.org/10.1016/j.jsg.2019.103975
Received 9 December 2019; Received in revised form 29 December 2019; Accepted 29 December 2019
Available online 2 January 2020

(Berkine) basin are situated at the south and north of Illizi basin (Boote et al., 1998; Klett, 2000). Fig. 1 represents the Illizi basin and studied well. This part of the Saharan platform tends to have a near flat structural dip and is thought to have been subject to the effects of strike-slip tectonics. Throughout the Paleozoic this basin has experienced several regressive and transgressive depositional cycle. Marine quartz arenites of glacial-tidal shallow marine origin deposited reservoir quality sands during Ordovician lowstand system tract. A major flooding event during Silurian deposited the source rocks (Aliev et al., 1971; Boudjema, 1987) with an average total organic carbon (TOC) content of 2–4% (Daniels and Emme, 1995). Prograding deltaic-fluvial and shallow marine/tidal sandstones of Devonian unit form the reservoir facies in Takouazet field, as encountered in the studied well. Devonian unit lies unconformably above the Silurian marine shale and it consists of marine or marginal marine sandstone members which are major hydrocarbon bearing formations in the studied field. These Devonian reservoir units are named as F6-A, B and C units. Various intraformational Paleozoic marine shales act as seals for reservoir facies in Illizi basin petroleum system (Van de Weerd and Ware, 1994; Boote et al., 1998). The studied well TAKW-1 in eastern Illizi basin encountered Devonian (F6) and Ordovician reservoirs. Fig. 2 represents the generalized lithostratigraphy of the Illizi basin.

3. Material and methods

3.1. Data used

The vertical discovery well TAKW-1 was drilled till 2675 m TVD (true vertical depth) in Takouazet field, eastern Illizi basin to explore the hydrocarbon potential in Paleozoic horizons. A complete set of conventional wireline logs (consisting of gamma ray, caliper, resistivity, compressional sonic slowness, bulk density and neutron porosity), FMI logs and direct downhole formation pressure measurements by Modular Dynamic Tool (MDT), leak-off test (LOT) data were available from the studied well. A quality check (QC) has been performed on the collected data before calculation stage. The brief workflow diagram for this present study has been presented in Fig. 3.

3.2. Estimation of rock mechanical properties

Rock elastic properties and rock strength parameters are critical inputs for geomechanical modeling. The standard practice is to estimate these properties from geophysical logs and calibrate the calculated dynamic values with static values available from core based measurements. In this study, we focused on four principal rock properties: Poisson's ratio (υ), Young's modulus (Y), coefficient of internal friction (μ) and Uniaxial Compressive strength (UCS).

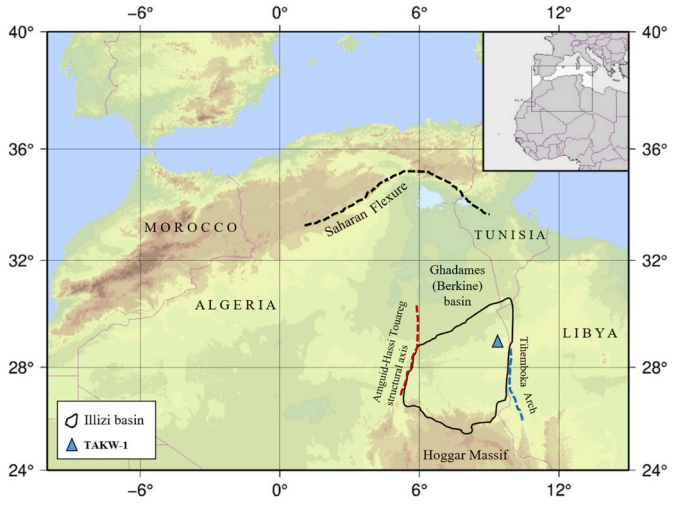

Fig. 1. Location of Illizi basin in North-Central Africa along with three structural trends. Studied well TAKW-1 has been presented as a triangle.

Dynamic rock elastic properties are calculated from density (RHOB), compressional wave velocity (Vp) and shear wave velocity (Vs) data. The equations are as below (Lal, 1999; Chang et al., 2006; Zoback, 2007):

$$\upsilon d = \frac{Vp^2 - 2Vs^2}{2(Vp^2 - Vs^2)} \tag{1}$$

$$Yd = RHOB^{*}Vs^2\left[\frac{3Vp^2 - 4Vs^2}{Vp^2 - Vs^2}\right] \tag{2}$$

$$\mu = tan\ \varphi \tag{3}$$

$$\varphi = \left[\ \mathrm{Sin}^{-1}\left(\frac{Vp - 1000}{Vp + 1000}\right)\right] \tag{4}$$

where υd and Yd are dynamic Poisson's ratio and Young's modulus respectively, φ is angle of internal friction (in degree) and μ is the coefficient of internal friction measured from logs. Vp and Vs are in meter/second unit. Chang et al. (2006) suggested an average value of 0.6 against frictional coefficient.

UCS has been estimated from compressional sonic slowness (DT). We have deployed two different UCS equations for sandstones and shales. McNally, 1987 propose following expression for fine grained, consolidated sandstones with wide range of porosity:

$$UCS_{Sandstone} = 122\ e^{-0.036\ DT} \tag{5}$$

For UCS calculation against shales, we used the following relationship by Horsrud (2001):

$$UCS_{Shale} = 0.77\left(\frac{304.8}{DT}\right)^{2.03} \tag{6}$$

where DT represents the sonic slowness log in us/ft unit and generated UCS is in mega-pascal (MPa) unit.

3.3. Orientation of maximum horizontal stress (S_H)

Approximately one fifth of the horizontal stress direction indicators is yielded by wellbore failures, as documented in World Stress Map (WSM) database (Sperner et al., 2003; Heidbach et al., 2016a, 2016b, 2018, 2019). When the circumferential radial stress concentration around the wellbore goes exceeds the tensile strength of the rock mass, wellbore fails parallel to S_H direction (Zoback, 2007) and this is known as drilling induced tensile fractures (DITF). In a vertical well FMI log, these tensile failures appear 180° apart as narrow conductive features parallel to wellbore axis (Heidbach et al., 2010; Tingay et al., 2008; Lai et al., 2018).

A cumulative 817 m of Palaeozoic section (2475-1658 m) covering the Devonian and Ordovician reservoirs have been logged by FMI tool. We interpreted the DITFs from the extensive FMI log and inferred S_H direction.

3.4. Vertical stress (S_v) magnitude

Density log data is conventionally used to estimate the overburden pressure, or vertical stress (S_v) and the equation is as follows:

$$Sv = \int_0^H RHOB^{*}g\ dH \tag{7}$$

where, RHOB is the bulk density log value at a depth (H), and g is gravitational acceleration.

Usually operators do not record wireline logs in the shallow parts as

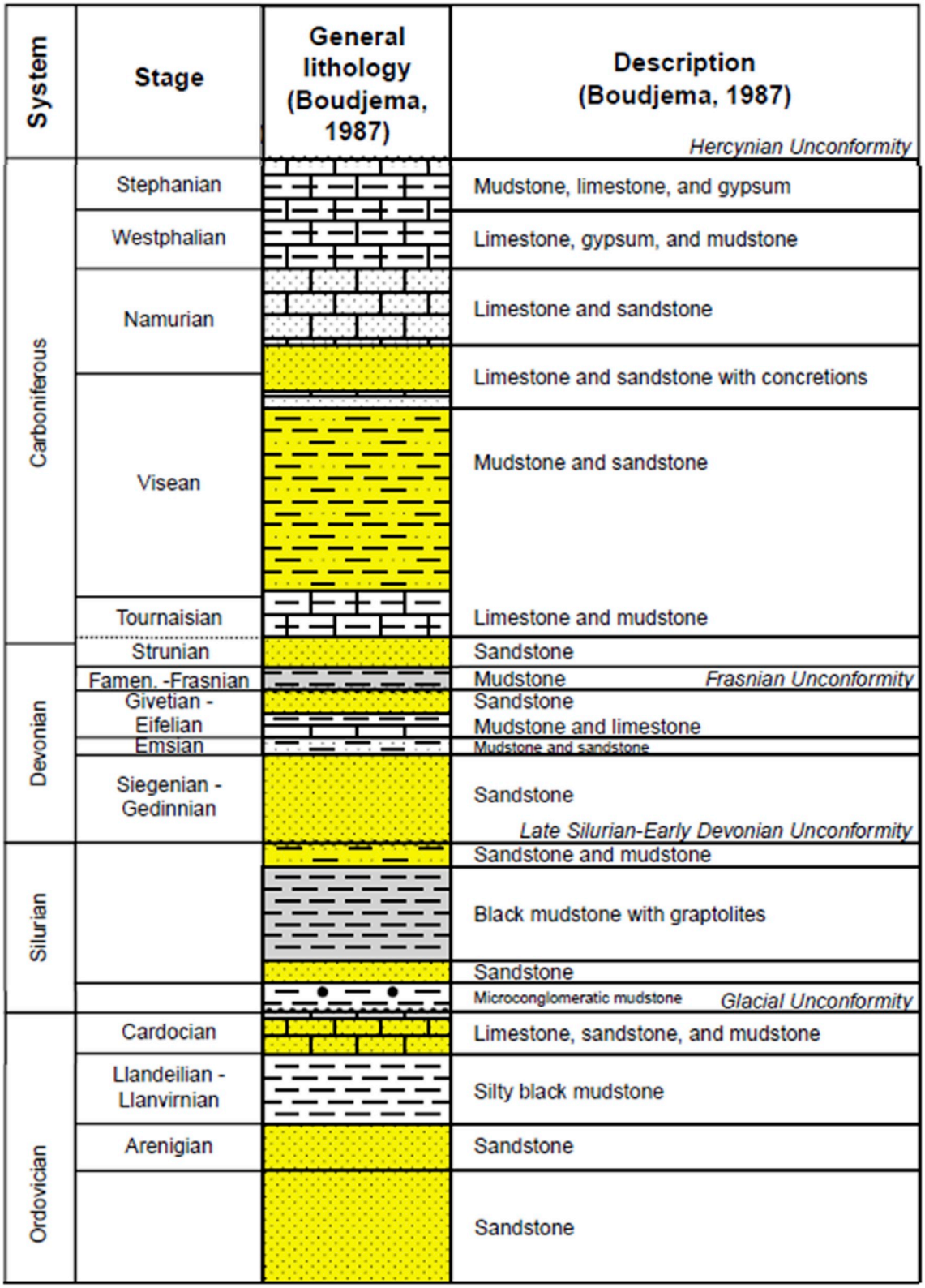

Fig. 2. Generalized lithostratigraphic column of Illizi basin, adapted from Boudjema (1987). The studied well TAKW-1 was drilled till Ordovician formation in Takouazet field, eastern Illizi basin.

its devoid of zone of interest and the second is to reduce the operating cost. In the interval of missing density at the shallower level, density was extrapolated using a power law curve using the following equation:

$$RHOB_{syn} = Rs + \left(\frac{TVD - AG}{3125}\right)^{\alpha} \quad (8)$$

where, $RHOB_{syn}$ is the synthetic density for shallow section, Rs is the

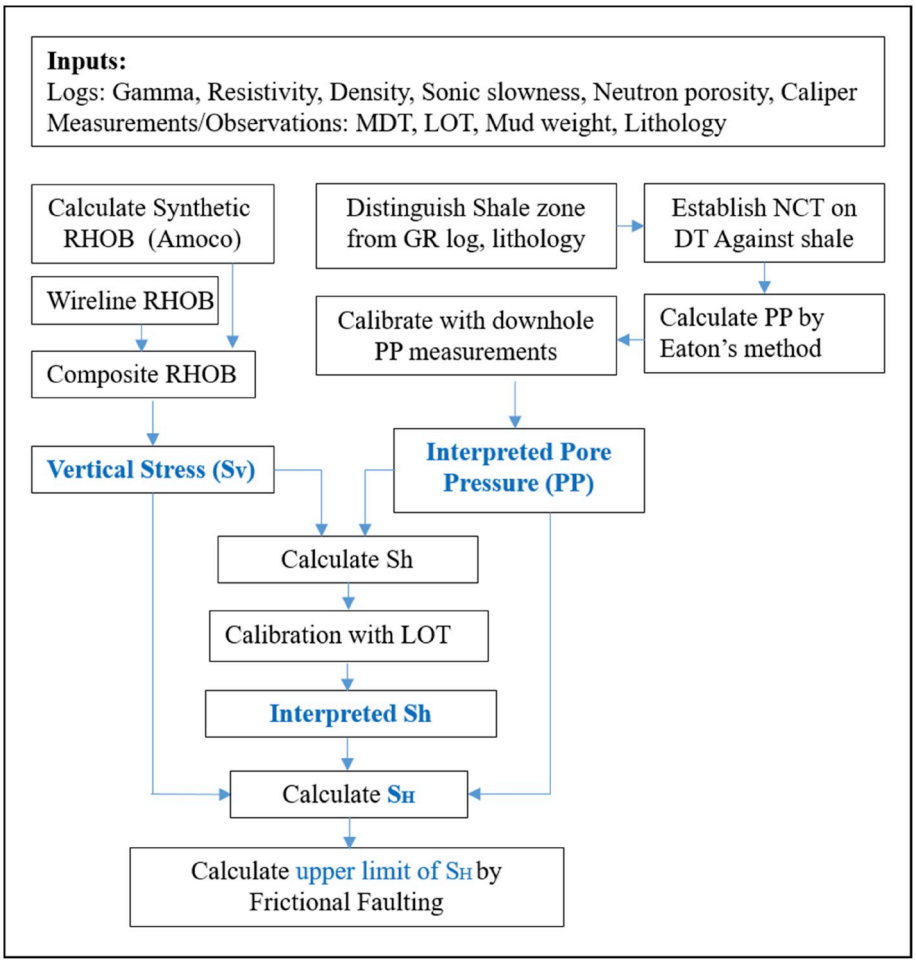

Fig. 3. Workflow diagram, as followed in this study.

surface sediment density (default value 1.9 g/cc), TVD is true vertical depth and AG is air gap (distance between drill floor and mean sea level). 'α' is a fitting parameter with default value of 0.6 (Radwan et al., 2019). The parameters of the power law curve were determined by adjusting the three reference points to match the power law curve to the density log over the depth interval for which density data was available (Sen et al., 2017).

We had looked for possible washed out segments in the borehole from caliper logs (Sen and Ganguli, 2019), since these are the potential zones where recorded RHOB can give erroneous data (as RHOB is measured using a padded tool) (Sen et al., 2015). Necessary environmental corrections have been introduced to nullify those bad data areas. Corrected composite density logs have been the input to estimate vertical stress using Eq. (1).

3.5. Pore pressure (PP) magnitude

Pore pressure (PP) is a critical parameter in Geomechanical model building, since S_h and S_H are dependent on PP. Presence of abnormal formation pressure can critically lower the effective stress values, which translates to reduced safe mud window, wellbore instability and hence drilling complexities. The commonly accepted industry practice is to estimate PP from indirect methods using geophysical logs (i.e. resistivity, sonic etc.) or drilling exponent and calibrate against the downhole measurements (which is only available against the reservoir units or potential hydrocarbon bearing zones) (Sen et al., 2018a, 2018b). To perform the indirect PP calculation method, first shale zones are distinguished from non-shale units using a combination of gamma ray, resistivity, neutron porosity and density logs along with drill cutting lithology information (Ramdhan and Goulty, 2011; Sen et al., 2019). Thereafter, a normal compaction trend (NCT) is established on the shale picks, which acts as the basis of PP characterization. A normally compacted shale indicates hydrostatic pressure regime, whereas any deviation from NCT would mean that the shale has higher pressure (Tingay et al., 2005; ; Zhang, 2011; Sen et al., 2020).

In this study, we have used compressional sonic slowness log and applied the widely accepted Eaton's equation (Eaton, 1975) as below:

$$PP = Sv - (Sv - Ph)*\left(\frac{DTCn}{DTC}\right)^3 \quad (9)$$

where Ph denotes hydrostatic pressure (approximately 0.433 psi/ft). DTC is the compressional sonic slowness log (us/ft) and DTCn is the sonic log response against shale.

Direct in-situ pore pressure measurements were available from principal reservoir formations. Downhole pressure data was recorded by Modular Formation Dynamics Tester tool, commonly known as MDT. This is a wireline tool that inserts a probe (single or dual probe module) into the target formation and a high precision pressure gauge records the formation pressure reading. This is also capable of reservoir fluid sampling. MDT data has been used for calibration of estimated PP in this study.

3.6. Minimum horizontal stress (S_h) magnitude

Leak-off test (LOT) provides the effective stress ratio (K), which translates to the ratio of the pressure at which formation fractures to the

value of Sv at that particular TVD. This 'K' parameter serves as the direct calibration point of S_h at the depth of interest. This effective stress ratio based approach to estimate Sh was proposed by Mathews and Kelly method (1967):

$$S_{hMK} = PP + K^*(Sv - PP) \quad (10)$$

where K is the effective stress coefficient and S_{hMK} is the estimated Sh from effective stress ratio.

Another approach for estimating S_h is poroelastic horizontal strain which involves tectonic strains to accommodate anisotropic horizontal stresses (Javani et al., 2017; Amiri et al., 2019), since tectonic strains applied to an elastic body of rock results in an addition of stress component (Najibi et al., 2017). The equation is as follows:

$$S_{hPoro} = \frac{\upsilon s}{1-\upsilon s}(Sv - PP) + PP + \upsilon s\frac{Ys}{1-\upsilon s^2}\varepsilon x + \frac{Ys}{1-\upsilon s^2}\varepsilon y \quad (11)$$

where S_{hPoro} is the minimum horizontal stress magnitude by strain model, υs is static Poisson's ratio; Ys is the static Young's modulus; εx and εy are two horizontal strain components along S_h and S_H directions (Najibi et al., 2017). εx and εy have been estimated by the equations below (Kidambi and Kumar, 2016):

$$\varepsilon x = Sv\frac{\upsilon s}{Ys}\left(\frac{1}{1-\upsilon} - 1\right) \quad (12)$$

$$\varepsilon y = Sv\frac{\upsilon s}{EYs\left(1 - \frac{\upsilon^2}{1-\upsilon}\right)} \quad (13)$$

Static values of elastic properties are measured on cores. Wang (2000) established the following relationship by to estimate static Poisson's ratio and Young's modulus from dynamic values:

$$\upsilon s = \upsilon d \quad (14)$$

$$Ys = 0.4142^*Yd - 1.0593 \quad (15)$$

where υd and Yd are dynamic Poisson's ratio and Young's modulus respectively.

In this study, we have utilized both the models - effective stress ratio as well as poroelastic strain model.

3.7. Maximum horizontal stress (S_H) magnitude

S_H magnitude is the most critical part of in-situ stress tensors, since it cannot be measured directly. However we have followed here the poroelastic strain model to estimate the S_H magnitude and the equation is as follows (Javani et al., 2017; Najibi et al., 2017):

$$SHMax_{poro} = \frac{\upsilon s}{1-\upsilon s}(Sv - PP) + PP + \upsilon s\frac{Ys}{1-\upsilon s^2}\varepsilon y + \frac{Ys}{1-\upsilon s^2}\varepsilon x \quad (16)$$

All the input parameters used in Eq. (12) have been described already in section 3.5.

Although there has not been a direct measurement of S_H like pore pressure, its upper limit can be constrained by frictional faulting theory (Brudy et al., 1997; Zoback, 2007). It states that the ratio of maximum (σ1) to minimum (σ3) effective principal stress can be correlated with a function of frictional coefficient factor (μ):

$$\frac{\sigma 1}{\sigma 3} = \frac{S1 - PP}{S3 - PP} = \left[\left(\mu^2 + 1\right)^{0.5} + \mu\right]^2 \quad (17)$$

S1 and S3 vary with the tectonic stress regime. For example, S_v is the highest principal stress in normal faulting regime, while lowest in reverse faulting regime based on Anderson's faulting principle. Townend and Zoback, 2000; Zoback, 2007 suggested an average value of 0.6 against μ.

4. Results and discussion

4.1. S_H orientation

We investigated the FMI log recorded against Devonian to Ordovician unit. Numerous DITF were identified and its orientations were interpreted, although wellbore breakouts could not be observed. WSM quality ranking policy suggests that C-quality stands for more than four distinct DITF segments with a combined length of ≥20 m in a single well and the standard deviation should be less than 25°, while more than 6 DITF zones of >40 m cumulative zones with ≤20° standard deviation defines a B-quality stress direction indicator (Heidbach et al., 2010). The highest quality is indicated a A-quality defined by ≥ 10 DITF zones with ≥100 m cumulative fracture length and ≤12° standard deviation (Heidbach et al., 2010; 2016a; 2016b; 2018; 2019).

In the studied well TAKW-1, DITFs occurred in the Ordovician interval. Seven distinguishable DITF zones have been observed between 2410 and 2462 m TVD (Fig. 4). The orientations of these DITFs are in between 140° and 160°N, with an average azimuth of 150°N (± 10°). Based on the observations from FMI logs, B-quality DITFs have been summarized that deciphers a NW orientation for S_H in the eastern Illizi basin.

We looked for S_H azimuth data from the adjacent areas and surrounding basins. All stress indicator data population in Algeria from WSM (Fig. 5) belongs to the north of Sahara flexure geographically and indicate a dominant NW-SE orientation. However various researchers (Koceir and Tiab, 2000; Patton et al., 2003; English et al., 2017; Paludan et al., 2017) worked out stress directions using wellbore failures from petroleum data of Ghadames (Berkine) basin, Ahnet basin, Hassi Messaoud area, Tiguentourine Field of southeastern Algeria etc. and confirmed a general S_H trend ranging between NNW and NW. These findings correlate strongly with our findings from Takouazet field, eastern Illizi basin. The overall NW-SE orientation of S_H translates to the relative plate motion of the African and Eurasian plates, which is in the same direction.

4.2. Magnitude of pore pressure and in-situ stress components

As the very first step of the workflow, S_v was determined from density log. For synthetic shallow density, we modeled three density profiles, using 'α' values as 0.6 (Default), 0.5 and 0.4. with a surface sediment density (Rs) of 1.9 g/cc (Eq. (8)). Based on the results (Fig. 6), α = 0.4 has been observed to be following the wireline density in best manner and hence used in calculation. A composite density combining shallow pseudo density and wireline bulk density had been used to generate vertical stress profile for the entire studied Palaeozoic stratigraphy. At the well TD (target depth) of 2476.5 m TVD, S_v has a magnitude of 8744.85 PSI, which reflects to 1.07 PSI/ft gradient in the onshore Takouazet field of eastern Illizi basin, Algeria. Interpreted Sv gradient and magnitude has been presented in Fig. 6.

PP has been calculated from sonic log and calibrated with downhole in-situ formation pressure measurements (MDT) available against Devonian and Ordovician reservoirs. Pore pressure distribution and the NCT have been presented in Fig. 7. Study reveals hydrostatic pressure regime from surface to the Devonian unit, which also includes Devonian F-6 sandstone reservoirs and an average pore pressure gradient of 0.47 PSI/ft has been interpreted in the mentioned interval. Deviation of sonic log response from NCT indicated the increase in formation pressure magnitude within Silurian shales. Fig. 7 clearly indicates an increase in neutron porosity log (NPHI) value against the Silurian shale. An abnormal pressure gradient of 0.66 PSI/ft continued till the base of Silurian unit at 2332 m TVD and the top of overpressure has been marked around 2100 m. Being deposited in shallow marine to marine system during a transgressive sea level condition, high sedimentation rate prevailed. As a result connate water could not escape from the pore spaces and failed to maintain a hydrostatic pressure head, thus exerting

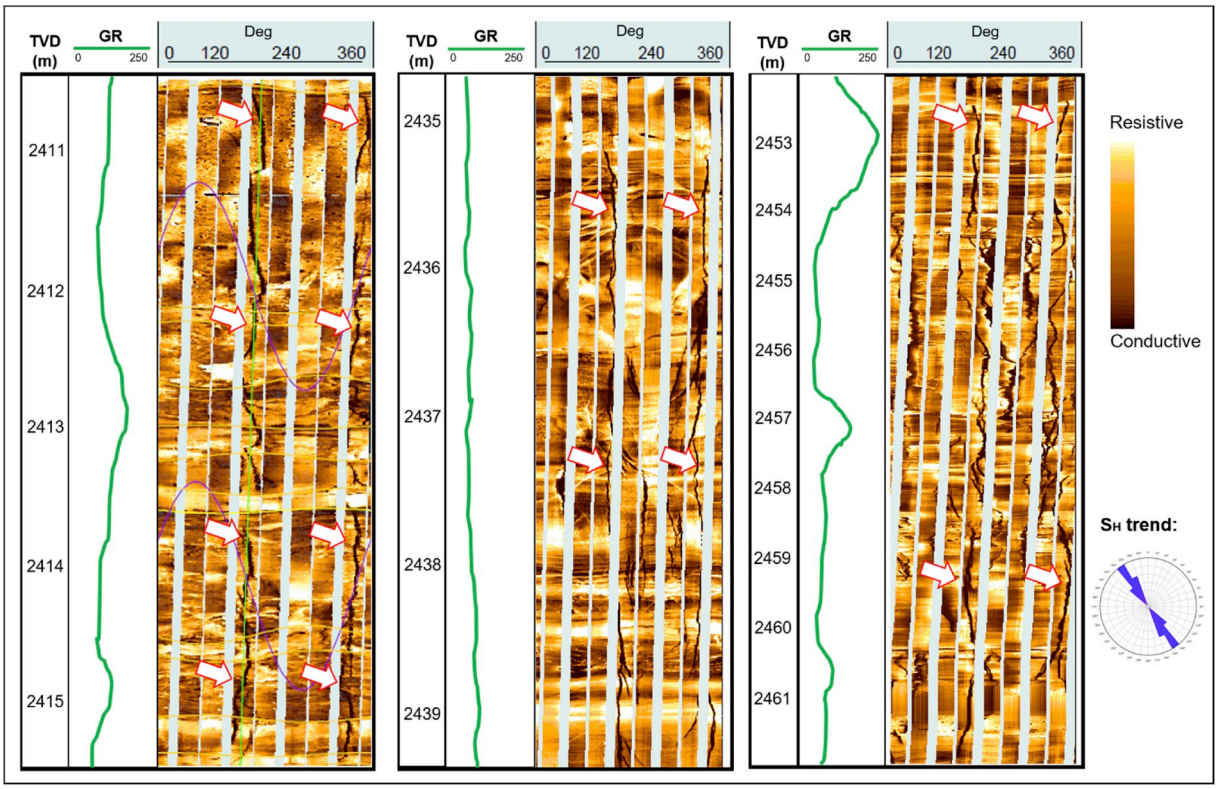

Fig. 4. Drilling Induced Tensile Fractures (DITF) interpreted from the FMI log (marked by arrows) against the Ordovician unit. A mean NW-SE orientation of S_H has been interpreted from these DITF, as presented in the rose plot.

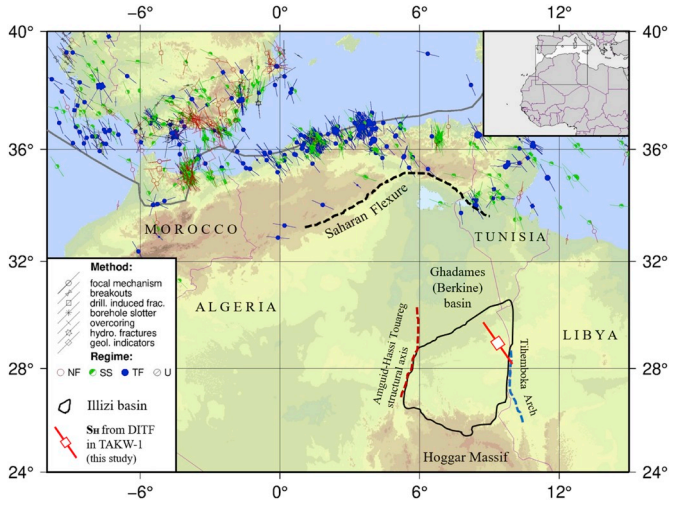

Fig. 5. Interpreted S_H orientation (150°N) from drilling induced tensile fractures (DITF) from the studied well (TAKW-1). Stress directions from northern Africa and European continents are from World Stress Map (WSM) database (Heidbach et al., 2016b; 2018, 2019).

abnormal pore pressure. Another critical aspect of the pressure distribution is the sudden drop in in-situ pore pressure from Silurian to Ordovician unit at around 2332 m TVD. The boundary between the two geological units is marked by a major unconformity across which the depositional system changes from regressive Lowstand System tract (Ordovician) to Transgressive System tract (Silurian). Ordovician unit reflects a normal pressure regime with a hydrostatic gradient (0.43 PSI/ft). The same has been confirmed by the MDT measurements against the reservoir sandstones (Fig. 7).

For the estimation of S_h, we have followed two approaches - poroelastic strain model and effective stress ratio. Poroelastic strain model for estimating horizontal stress magnitudes require the characterization of rock elastic properties. Based on density, compressional and shear sonic logs, we estimated dynamic elastic moduli, i.e. Young's modulus, Poisson's ratio as well as rock strength, i.e. Uniaxial Compressive strength (UCS) (Fig. 8). Result shows an average 107–150 MPa UCS against Ordovician sandstones, which correlates strongly with the core based uniaxial measurements of the same formation from southern Illizi basin, where a UCS range of 90.38–163.96 MPa has been reported by English et al. (2017). Young's modulus values of overpressured lower Silurian shale and Ordovician units are 6–10 MPa and 37–50 MPa respectively, while English et al. (2017) gave similar values from south Illizi basin cores (7–8 MPa for lower Silurian shale and 41–69 MPa range for various Ordovician reservoir units). Based on the dynamic rock mechanical properties followed by dynamic to static property calibration (Eqs. (8) and (9); Wang, 2000), Sh has been estimated for the Paleozoic section and presented in Fig. 9. The second approach of Sh estimation employs leak-off test (LOT). A leak-off test was carried out at 1670 m TVD (against Devonian shale) to understand the downhole pressure limit that creates a fracture in the formation for the fluid to leak through. An effective stress ratio of 0.6 has been interpreted from the LOT test, which provides us a S_h estimate (Fig. 9). Patton et al. (2003) also reported a very close effective stress ratio value (0.59) from the Tiguentourine field in Illizi basin. Based on the magnitudes of both Sh models (Table 1), normally pressured Devonian unit reveals a Sh range between 0.74 and 0.81 PSI/ft; abnormally pressured Silurian shales reflect a high Sh gradient of 0.86–0.88 PSI/ft, whereas Ordovician unit sandstones and shales display 0.68 and 0.78 PSI/ft respectively. S_H magnitude based on poroelastic strain model has been presented in Fig. 9 and Table 1. Based on the poroelastic model approach, S_H has an average gradient of 1.14 PSI/ft in the Devonian unit. With the increase in PP against Silurian shale, S_H magnitude increases and a maximum 1.34 PSI/ft gradient has been recorded in overpressured Silurian shale. Ordovician unit reveals

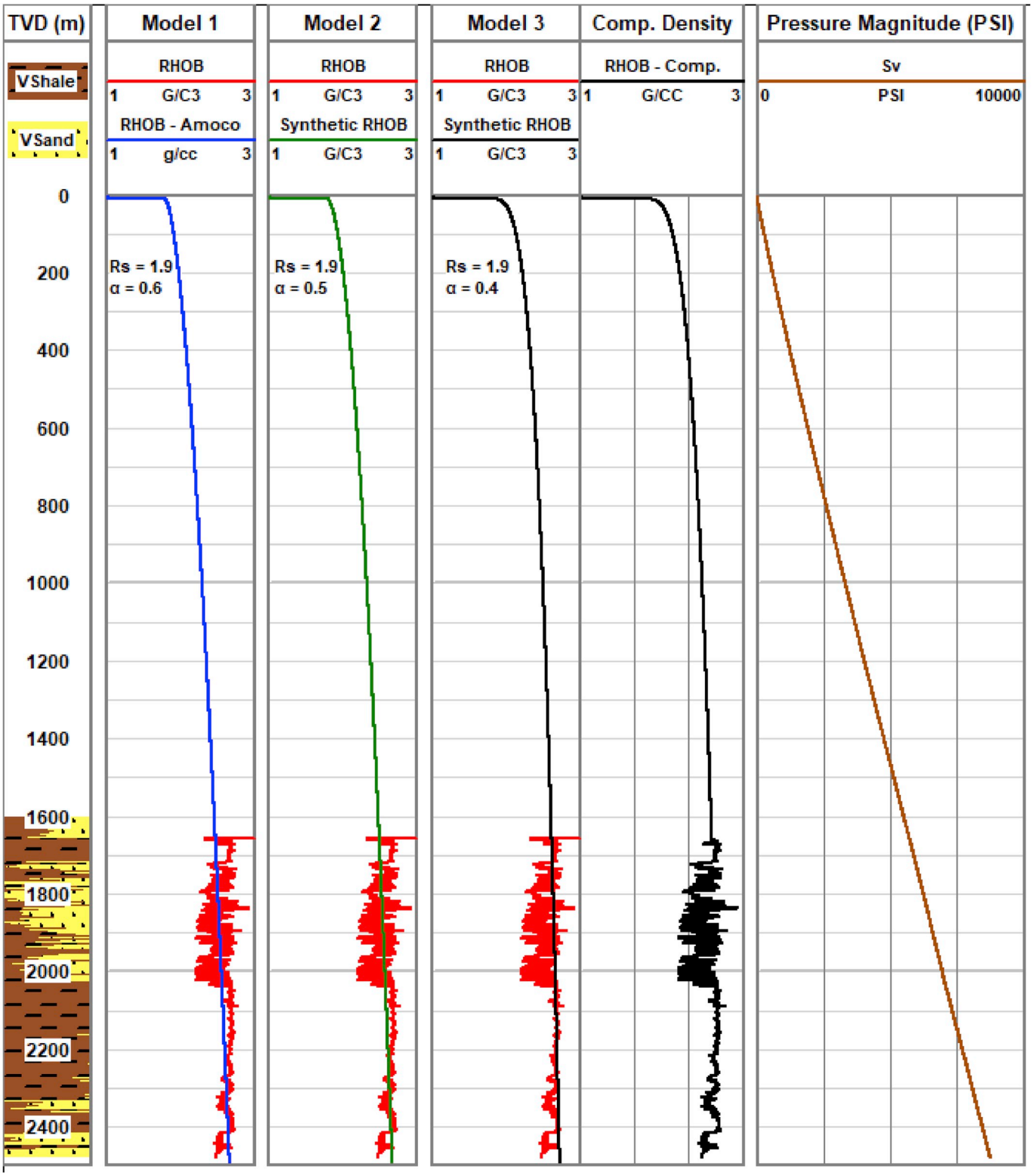

Fig. 6. Synthetic density curve with modified Amoco coefficients (Rs = 1.9 g/cc, α = 0.4, Track 4) follows the wireline density (red) trend better. Interpreted vertical stress (Sv) from composite density profile (black curve on Track 5) has been presented on Track 6.

an average 1.12 PSI/ft gradient.

4.3. Stress regime

Interpreted in-situ stress magnitudes have been presented in Fig. 9 and Table 1, which reveals S_H is the maximum magnitude, while S_h is the least principal stress ($S_H > Sv > S_h$) in the eastern Illizi basin. Based on Andersonian classification, the study area indicates a strike-slip faulting regime. S_H/S_v ratio varies between 1.01 and 1.26. Patton et al. (2003) reported a S_H/S_v ratio of 1.04 from southeastern Algeria. A cross plot between S_v normalized minimum and maximum horizontal stress components (Fig. 10) depicts this vertical change in in-situ stress state.

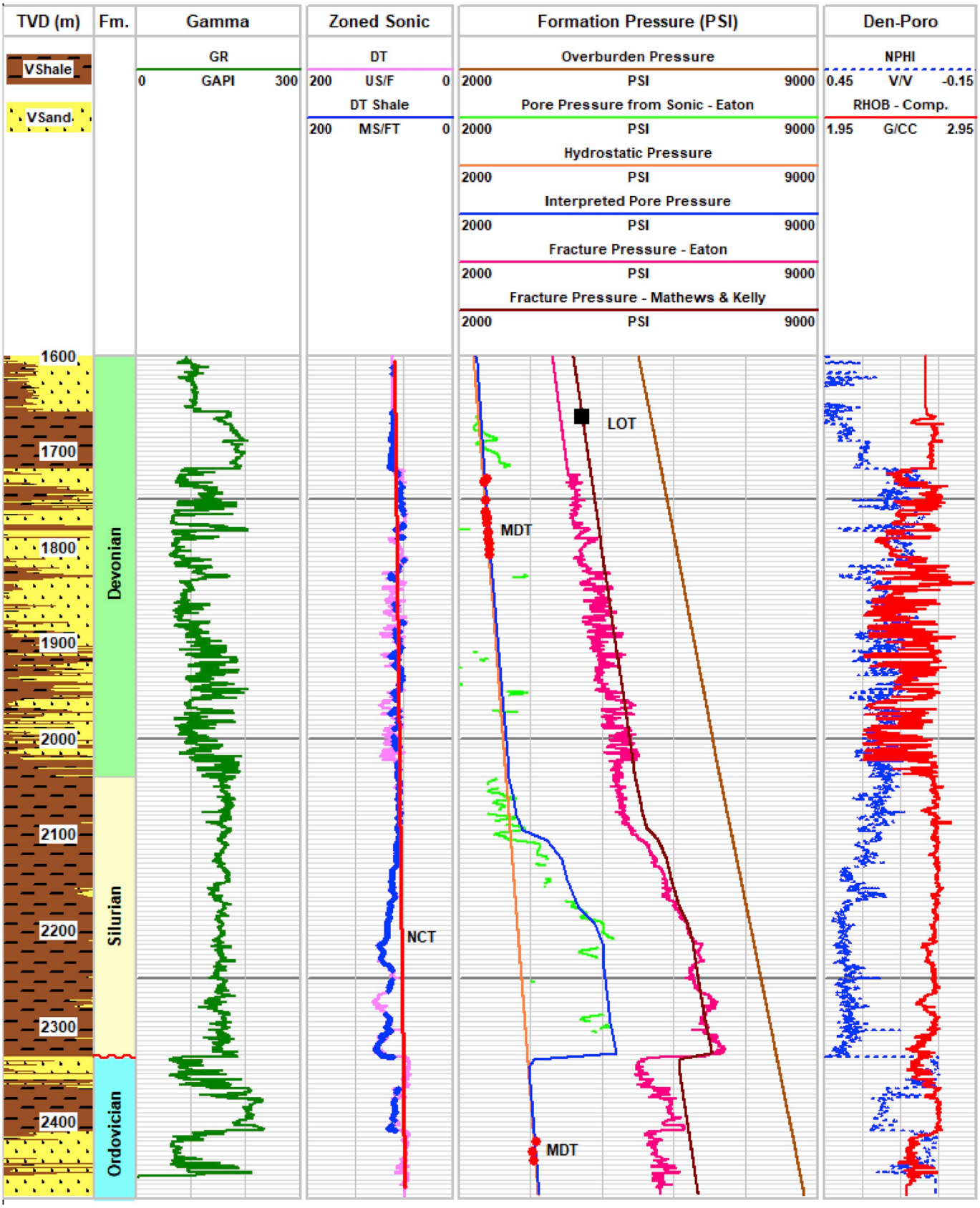

Fig. 7. Represents NCT on DT log (Track 4) used to estimate pore pressure (PP) profile. PP against Devonian and Ordovician reservoirs have been interpreted from MDT data.

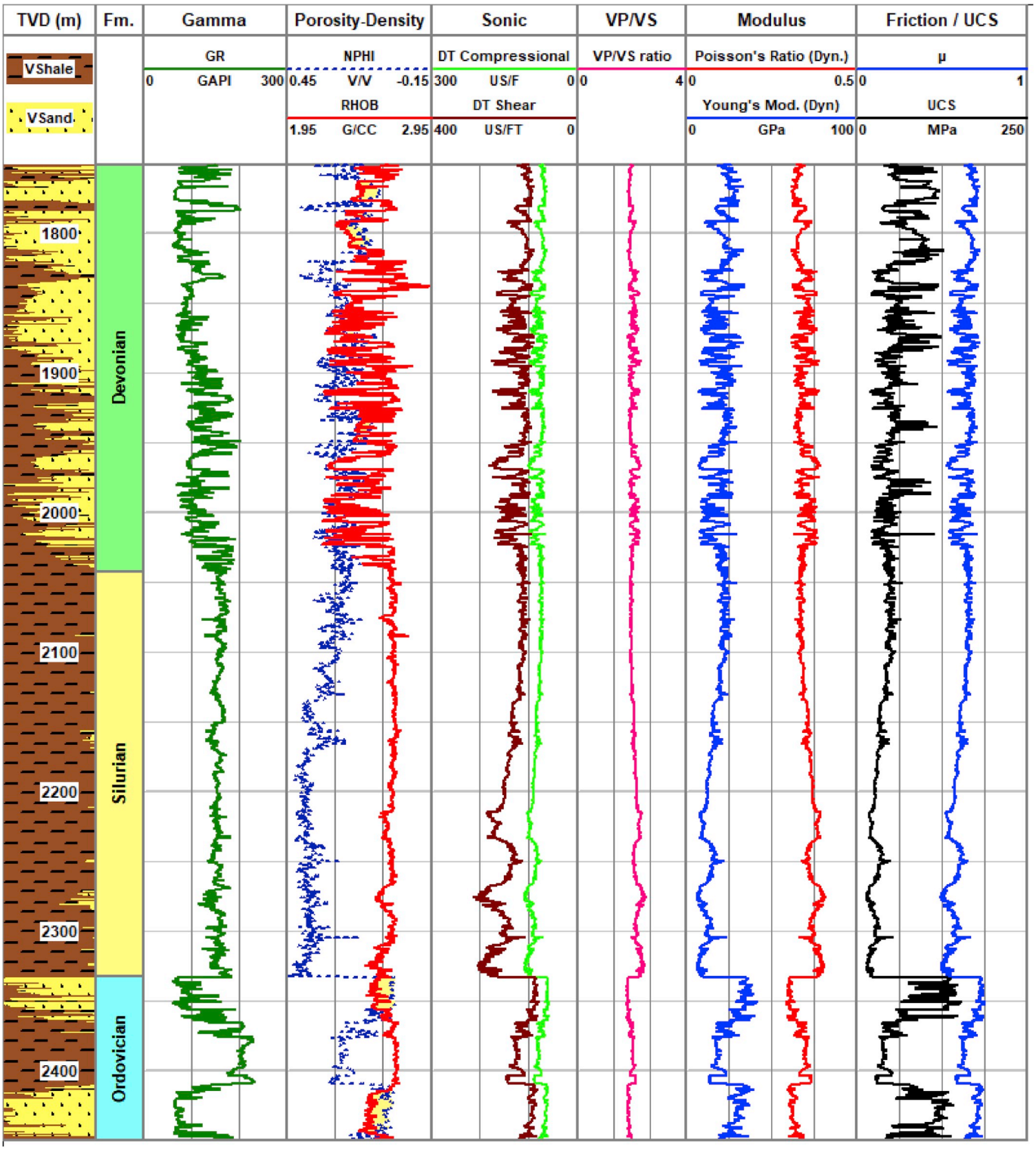

Fig. 8. Represents estimated dynamic elastic parameters and rock strength parameters from the studied well.

Based on frictional faulting theory (Zoback, 2007; Zoback, 2007), we have estimated the upper bound of SH in the study area using Eq. (13) considering a strike slip regime (S1=S_H, S3=S_h and $\mu = 0.6$). The output has been presented in Fig. 9 and Table 1. Since frictional faulting limit is based on the effective maximum and minimum principal stress ratio, a decrease in the S_H upper limit magnitude has been observed against the abnormally pressured Silurian shale (Fig. 9).

4.4. *Fault reactivation potential*

Hydraulic fracturing and fluid injection can potentially induce local seismicity by affecting the stress field (Tingay et al., 2005) and it can result in fault reactivation (Townend and Zoback, 2000; Moeck and Backers, 2011; Reis et al., 2013). We evaluated the fault reactivation chances at two primary reservoir levels, i.e. Devonian and Ordovician, where hydraulic stimulation might be attempted for enhanced

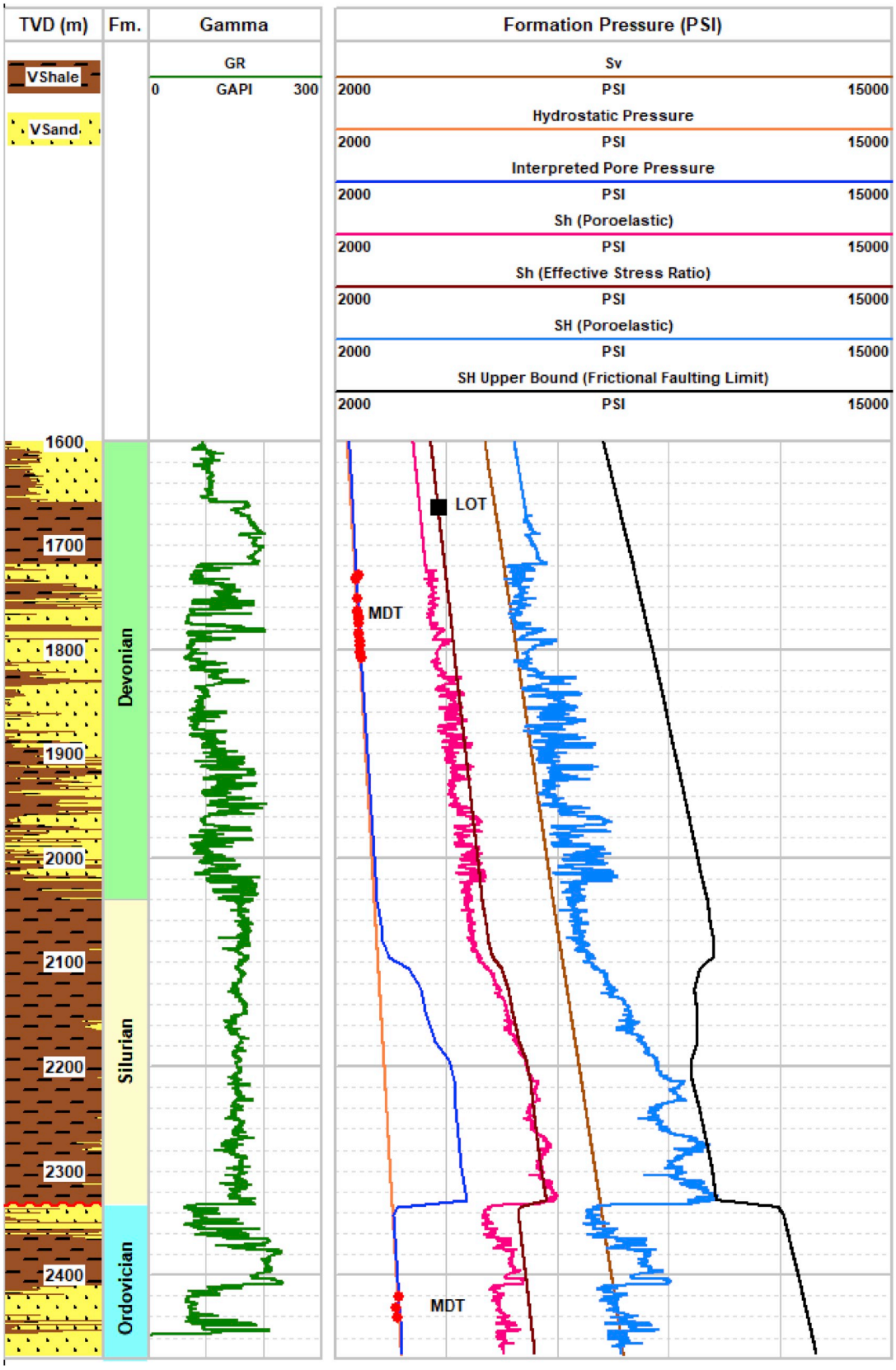

Fig. 9. Represents interpreted principal stress components and pore pressure in the studied well. Minimum horizontal stress (S_h) estimated from Effective stress ratio and poroelastic strain models. Maximum horizontal stress (S_H) magnitude calculated from poroelastic strains, whereas an upper bound has been constrained from Frictional faulting limit.

Table 1
Interpreted pore pressure (PP) and principal in-situ stress (S_v, S_h and S_H) magnitudes across the Paleozoic stratigraphy.

TVD (m)	Age	Pressure Magnitude (PSI)							Comments
		S_v	PP	PP Regime	S_h		S_H	S_H Bound	
					Poroelastic	Eff. Stress Ratio			
1700	Devonian	5885.5	2442.9	Normal (Hydrostatic)	4080.5	4521.1	6658.4	8860.2	F-6 Reservoir
1800		6248.5	2586.8		4447.6	4789.9	6620.7	9428.4	
1900		6603.2	2730.5		4792.7	5065.9	7191.7	9952.1	
2000		6662.5	2874.2		5272.7	5344.5	8051.4	10478.3	
2050		7139.7	2945.9		4966.8	5487.8	7289.4	10740.5	
2100	Silurian	7330.4	3717.8	Overpressure	5388.6	5785.3	7863.9	10697.6	Pressure Ramp
2150		7521.8	4124.5		6059.3	6171.2	8921.1	10465.9	
2200		7713.1	4685.8		6496.6	6507.9	9560.1	10339.8	
2300		8090.9	4959.5		6840.8	6837.3	10080.3	10823.7	Continuous Overpressure
2330		8202.8	5081.9		6907.1	6943.8	10396.1	11289.2	
2340	Ordovician	8239.7	3362.5	Normal (Hydrostatic)	5526.3	6311.2	7999.1	12442.9	Ordovician IV-2 and IV-1 Reservoirs
2370		8351.3	3405.8		5957.3	6379.1	8913.9	12648.8	
2400		8466.4	3448.8		6394.8	6466.3	9696.9	12826.5	
2450		8650.2	3520.9		6039.4	6605.4	8953.8	13107.5	
2476		8743.3	3558.1		5944.6	6675.1	8703.8	13247.8	

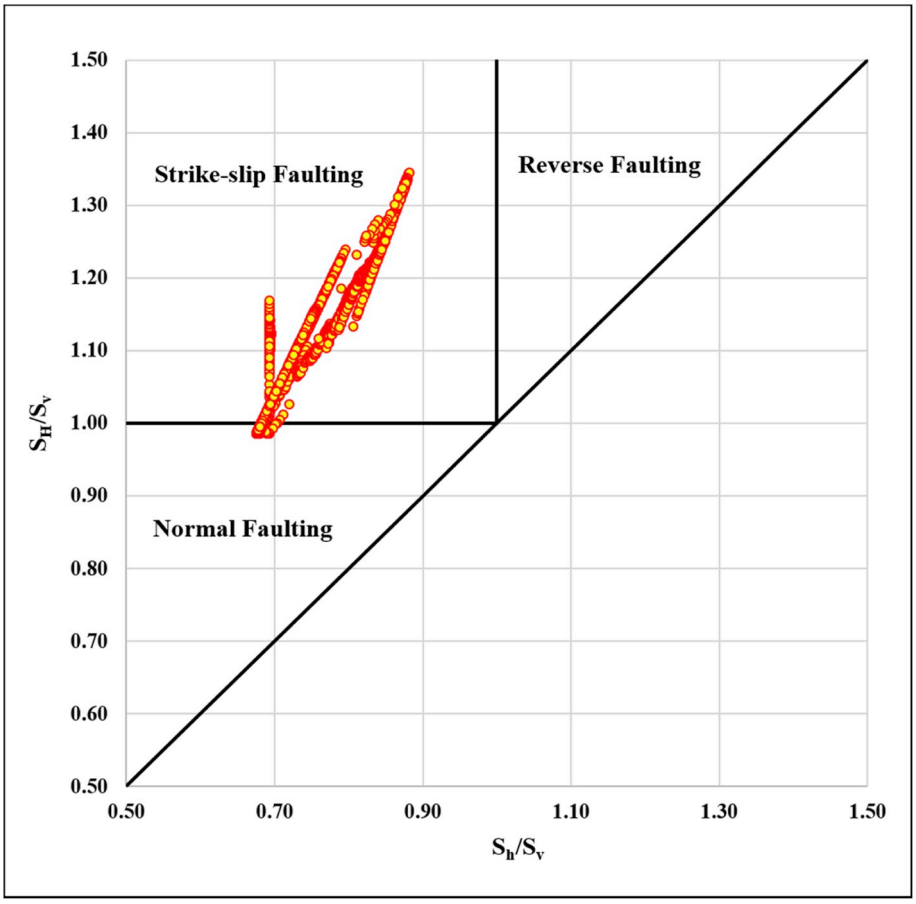

Fig. 10. Represents the crossplot between principal horizontal stress magnitudes normalized with vertical stress (S_v) from the studied well, indicating Strike-slip faulting regime in the eastern Illizi basin (S_H/S_v >1).

production. Stress polygons based on frictional faulting theory has been presented in Fig. 11 at 1765 m and 2440 m, which belongs to Devonian F6 and Ordovician IV reservoirs respectively. At 1765 m, reservoir zone F6 has a S_v of 6125 PSI, pore pressure from downhole measurements yielded a value of 2540 PSI (hydrostatic) and effective stress ratio provided S_h magnitude of 4701 PSI. S_v, PP and S_h values at Ordovician IV reservoir level has been estimated as 8614 PSI, 3507 PSI and 6578 PSI respectively. Rock mechanical property characterization provided average UCS values of 115 and 125 MPa at these two reservoirs (Fig. 11). Poroelastic strain model estimated S_H magnitude of 7100 and 9560 PSI respectively for Devonian and Ordovician units. At present day condition, both the dataset falls into strike-slip faulting polygon.

Frictional faulting theory assumes effective stress ratio controls the shear slippage of critically stressed faults. So if pore pressure increases by hydraulic fracturing fluid injection, effective stress reduces, stress polygons squeeze (Fig. 11) and it might result in fault slip. Based on present day in-situ stress distribution and hydrostatic formation pore pressure condition, significant pore pressure increments are required at

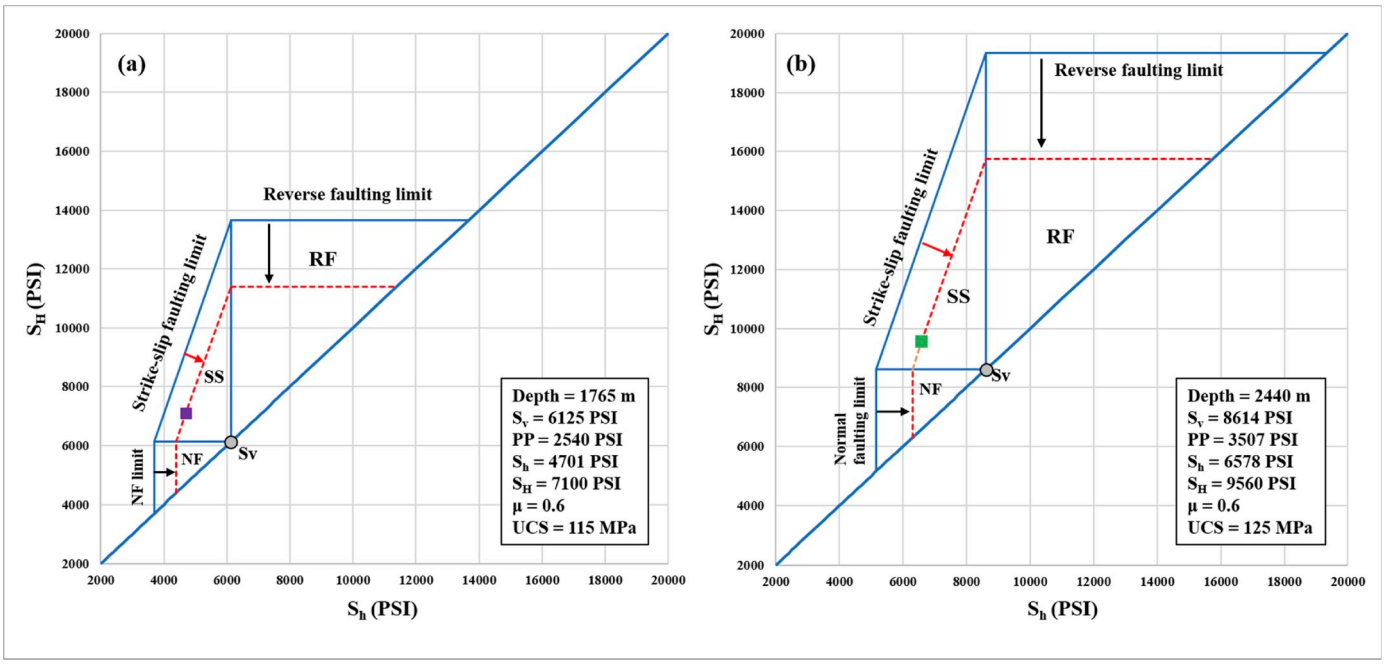

Fig. 11. Stress polygons: in-situ stress data from the studied well at the **(a)** Devonian reservoir level, 1765 m TVD (violet square) and **(b)** Ordovician reservoir level, 2440 m TVD (green square). Frictional faulting limits for three possible stress polygons (normal, strike-slip and reverse faulting regimes) have been plotted along with. Present stress state plotted in the stress polygon indicates Strike-slip faulting in both the reservoirs. The small/squeezed stress polygon marked by dotted red lines present the effect of pore pressure increase. Arrow indicates the result of pore pressure increment causing fault reactivation (shear slippage) and induced seismicity at Devonian F6 and Ordovician IV reservoirs.

Devonian and Ordovician reservoirs to reactivate an existing critically oriented fault.

5. Conclusion

A comprehensive geomechanical model has been presented from the studied TAKW-1 well, drilled in eastern Illizi basin, Algeria to ascertain the magnitude of pore pressure, principal in-situ stress components and orientation of horizontal stress. An integration of geophysical logs, downhole measurements (leak-off pressure and formation pressure by MDT) has been used to estimate formation pressure magnitudes and rock elastic properties. Silurian shale has been interpreted to be abnormally pressured, whereas the Devonian and Ordovician units consisting of hydrocarbon bearing sandstones indicate normal pore pressure (hydrostatic regime). Drilling induced tensile fractures from image log deciphered a NW-SE trend for maximum horizontal stress. Based on the relative stress magnitudes, a strike-slip normal faulting has been observed in the studied eastern Illizi basin. We deployed stress polygon approach to decipher the fault reactivation potential by pore pressure increase during hydraulic stimulation at the two major reservoir level (Devonian and Ordovician units). Results quantified the required minimum pore pressure increment to cause a fault slip at the both primary hydrocarbon bearing zones.

The workflow adopted in this paper can be extended as a standard practice to establish basinal stress regime and quantify shear slippage potential from 1D geomechanical model. This can be very useful in building field development plan (FDP) by precise placement of deviated well and subsequent optimum hydraulic fracturing design.

Declaration of competing interest

The authors declare that they have no known competing financial interests or personal relationships that could have appeared to influence the work reported in this paper.

CRediT authorship contribution statement

Rafik Baouche: Data curation, Supervision, Project administration, Writing - review & editing. **Souvik Sen:** Conceptualization, Formal analysis, Methodology, Software, Validation, Visualization, Writing - original draft, Writing - review & editing. **Khadidja Boutaleb:** Resources, Writing - review & editing.

Acknowledgement

Authors are grateful to Ian Alsop, Editor, Journal of Structural Geology and the two reviewers for their reviews and comments, that benefited the manuscript. Authors would like to thank Sonatrach Exploration Company South field, Algeria for providing the dataset and permission to publish this work. SS expresses his sincere gratitude to Geologix Limited for giving access to Pore Pressure and Geomechanics module of GEO Suite of software, which has been instrumental for all the calculation and analyses documented in this study. Interpretation presented here are solely of authors and do not necessarily reflect their organizations.

References

Aliev, M., Aït Laoussine, N.A., Avrov, V., Aleksine, G., Barouline, G., Iakovlev, B., Korj, M., Kouvykine, J., Makarov, V., Mazanov, V., Medvedev, E., Mkrtchiane, O., Moustafinov, R., Oriev, L., Oroudjeva, D., Oulmi, M., Saïd, A., 1971. Geological Structures and Estimation of Oil and Gas in the Sahara in Algeria: Spain. Altamira-Rotopress, S.A., p. 265

Amiri, M., Lashkaripour, G.R., Ghabezloo, S., Moghaddas, N.H., Tajareh, M.H., 2019. Mechanical earth modeling and fault reactivation analysis for CO_2 enhanced oil recovery in Gachsaran oil field, south-west of Iran. Environ. Earth Sci. 78 (112).

Boote, D.R.D., Clark-Lowes, D.D., Traut, M.W., 1998. Palaeozoic petroleum systems of north Africa. In: Macgregor, D.S., Moody, R.T.J., Clark-Lowes, D.D. (Eds.), Petroleum Geology of North Africa, vol. 132. Geological Society, London, Special Publication, pp. 7–68.

Boudjema, A., 1987. Evolution structurale du bassin petrolier «Triasique» du Sahara Nord Oriental (Algerie): Thèse a l'Université de Paris-Sud. Centre d'Orsay, p. 290.

Brudy, M., Zoback, M.D., Fuchs, K., Rummel, F., Baumgartner, J., 1997. Estimation of the complete stress tensor to 8 km depth in the KTB scientific drill holes : implications for crustal strength. J. Geophys. Res. 102 (B8), 18453–18475.
Chang, C., Zoback, M.D., Khaskar, A., 2006. Empirical relations between rock strength and physical properties in sedimentary rocks. J. Pet. Sci. Eng. 51, 223–237.
Daniels, R.P., Emme, J.J., 1995. Petroleum system model, eastern Algeria, from source rock to accumulation; when, where, and how? Proceedings of the Seminar on Source Rocks and Hydrocarbon Habitat in Tunisia. Entrep. Tunis. Activités Petrolieres Mem. 9, 101–124.
Eaton, B.A., 1975. The equation for geopressure prediction from well logs. In: In: Fall Meeting of the Society of Petroleum Engineers of AIME, Dallas, TX, USA September 28-October 1.
English, J.M., Finkbeiner, T., English, K.L., Cherif, R.Y., 2017. State of Stress in Exhumed Basins and Implications for Fluid Flow: Insights from the Illizi Basin, Algeria, vol. 458. Geological Society, London, Special Publications, pp. 89–112.
Heidbach, O., Rajabi, M., Reiter, K., Ziegler, M., 2016b. World Stress Map 2016. GFZ Data Services.
Heidbach, O., Rajabi, M., Reiter, K., Ziegler, M.O., 2019. World stress map. In: Sorkhabi, R. (Ed.), Encyclopedia of Petroleum Geoscience. Encyclopedia of Earth Sciences Series. Springer, Cham.
Heidbach, O., Barth, A., Müller, B., Reinecker, J., Stephansson, O., Tingay, M., Zang, A., 2016a. WSM Quality Ranking Scheme, Database Description and Analysis Guidelines for Stress Indicator. World Stress Map Technical Report 16-01. GFZ German Research Centre for Geosciences.
Heidbach, O., Rajabi, M., Cui, X., Fuchs, K., Müller, B., Reinecker, J., Reiter, K., Tingay, M., Wenzel, F., Xie, F., Ziegler, M.O., Zoback, M.-L., Zoback, M.D., 2018. The World Stress Map database release 2016: crustal stress pattern across scales. Tectonophysics 744, 484–498.
Heidbach, O., Tingay, M., Barth, A., Reinecker, J., Kurfeß, D., Müller, B., 2010. Global crustal stress pattern based on the World Stress Map database release 2008. Tectonophysics 482, 3–15.
Hoesni, M.J., 2004. The Origin of Overpressure in the Malay Basin and its Influence on Petroleum Systems. Ph.D. thesis, University of Durham.
Horsrud, P., 2001. Estimating mechanical properties of shale from empirical correlations. SPE Drill. Complet. 16 (2), 68–73.
Javani, D., Aadnoy, B., Rastegarnia, M., Nadimi, S., Aghighi, M.A., Maleki, B., 2017. Failure criterion effect on solid production and selection of completion solution. J. Rock Mech. Eng. Geotech. Eng. 9, 1123–1130.
Kidambi, T., Kumar, G.S., 2016. Mechanical Earth Modeling for a vertical well drilled in a naturally fractured tight carbonate gas reservoir in the Persian Gulf. J. Pet. Sci. Eng. 141, 38–51.
Klett, T.R., 2000. Total Petroleum Systems of the Illizi Province, Algeria and Libya – Tanezzuft-Illizi. U.S. Geological Survey Bulletin 2022-A.
Koceir, M., Tiab, D., 2000. Influence of Stress and Lithology on Hydraulic Fracturing in Hassi Messaoud Reservoir, Algeria. SPE/AAPG Western Regional Meeting, Long Beach, CA, USA. June 19-22, SPE-62608-MS.
Lai, J., Wang, G., Wang, S., Cao, J., Li, M., Pang, X., Han, C., Fan, X., Yang, L., He, Z., Qin, Z., 2018. A review on the applications of image logs in structural analysis and sedimentary characterization. Mar. Pet. Geol. 95, 139–166.
Lal, M., 1999. Shale stability: drilling fluid interaction and shale strength. In: SPE Latin American and Caribbean Petroleum Engineering Conference. Caracas Venezuela. April 21-23.
McNally, G.H.N., 1987. Estimation of coal measures rock strength using sonic and neutron logs. Geoexploration 24, 381–395.
Meng, Z., Zhang, J., Wang, R., 2011. In-situ stress, pore pressure and stress dependent permeability in the Southern Qinshui Basin. Int. J. Rock Mech. Min. Sci. 48 (1), 122–131.
Moeck, I., Backers, T., 2011. Fault reactivation potential as a critical factor during reservoir stimulation. First Break 29, 73–80.
Najibi, A.R., Ghafoori, M., Lashkaripour, G.R., Asef, M.R., 2017. Reservoir geomechanical modeling: In-situ stress, pore pressure, and mud design. J. Pet. Sci. Eng. 151, 31–39.
Paludan, J., Kerrouche, N., Toufik, H., Belahmeur, S., 2017. In: The State of Stress in North Africa - A Conceptual Model Based on Borehole Image Data from Algerian Oil Wells. Second EAGE Borehole Geology Workshop. Oct 9-11.
Patton, T.L., Batchelor, A.S., Foxford, K.A., Hellman, T.J., Maache, N., 2003. AAPG Hedberg Conference, Paleozoic and Triassic Petroleum Systems in North Africa. In: In Situ Stress State –Tiguentourine Field, Southeastern Algeria. Algiers, Algeria, Feb 18-20.
Rajabi, M., Tingay, M., Heidbach, O., 2016. The present-day state of tectonic stress in the Darling Basin, Australia: implications for exploration and production. Mar. Pet. Geol. 77, 776–790.
Radwan, A.E., Abudeif, A.M., Attia, M.M., Mohammed, M.A., 2019. Pore and fracture pressure modeling using direct and indirect methods in Badri Field, Gulf of Suez, Egypt. J. Afr. Earth Sci. 156, 133–143.
Ramdhan, A.M., Goulty, N.R., 2011. Overpressure and mudrock compaction in the Lower Kutai Basin, Indonesia: a radical reappraisal. AAPG (Am. Assoc. Pet. Geol.) Bull. 95, 1725–1744.
Reis, A., Bezerra, F.H., Ferreira, J.M., Nascimento, A.F.do, Lima, C.C., 2013. Stress magnitude and orientation in the Potiguar Basin, Brazil: implications on faulting style and reactivation. J. Geophys. Res. Solid Earth 118, 1–14.
Sayers, C.M., Johnson, G.M., Denyer, G., 2002. Predrill pore-pressure prediction using seismic data. Geophysics 67 (4), 1286–1292.
Sen, S., Corless, J., Dasgupta, S., Maxwell, C., Kumar, M., 2017. Issues faced while calculating overburden gradient and picking shale zone to predict pore pressure. In: In: 1st EAGE Workshop on Pore Pressure Prediction, Pau, France March 19-21.
Sen, S., Ganguli, S.S., 2019. Estimation of pore pressure and fracture gradient in volve field, Norwegian north sea. In: SPE Oil and Gas India Conference and Exhibition. Mumbai, India, April 9-11.
Sen, S., Ghosh, I., Kumar, M., 2015. Uncertainty in well log analyses and petrophysical interpretationsUncertainty in well log analyses and petrophysical interpretations. In: 11th Biennial International Conference & Exposition, SPG, Jaipur, India, December 4-6.
Sen, S., Kundan, A., Kalpande, V., Kumar, M., 2019. The present-day state of tectonic stress in the offshore Kutch-Saurashtra Basin, India. Mar. Pet. Geol. 102, 751–758.
Sen, S., Kundan, A., Kumar, M., 2018a. Post-drill analysis of pore pressure and fracture gradient from well logs and drilling events – an integrated case study of a high pressure exploratory well from Panna East, Mumbai Offshore basin, India. In: In: Pore Pressure and Geomechanics from Exploration to Abandonment, AAPG Geosciences Technology Workshop, Perth, Australia, June 6-7.
Sen, S., Kundan, A., Kumar, M., 2020. Modeling Pore Pressure, Fracture Pressure and Collapse Pressure Gradients in Offshore Panna, Western India: Implications for Drilling and Wellbore Stability. Natural Resources Research. https://doi.org/10.1007/s11053-019-09610-5.
Sen, S., Maxwell, C., Kumar, M., 2018b. Real Time Pore Pressure Interpretation from Drilling Events – A Case Study from High Pressure Offshore Exploratory Well. In: In: Operations Geoscience Adding Value, The Geological Society, London, November 7-8.
Sperner, B., Müller, B., Heidbach, O., Delvaux, D., Reinecker, J., Fuchs, K., 2003. Tectonic stress in the earth's crust: advances in the world stress map Project. In: Nieuwland, D. (Ed.), New Insights into Structural Interpretation and Modelling, vol. 212. Geol. Soc. Lond. Spec. Publ., pp. 101–116
Tingay, M., Müller, B., Reinecker, J., Heidbach, O., Wenzel, F., Fleckenstein, P., 2005. Understanding tectonic stress in the oil patch: the World stress map Project. Lead. Edge 24, 1276–1282.
Tingay, M., Reinecker, J., Muller, B., 2008. Borehole breakout and drilling -induced fracture analysis from image logs. World Stress Map Project Guidelines: Image Logs.
Tingay, M.R., Hillis, R.R., Morley, C.K., King, R.C., Swarbrick, R.E., Damit, A.R., 2009. Present-day stress and neotectonics of Brunei: implications for petroleum exploration and production. AAPG (Am. Assoc. Pet. Geol.) Bull. 93, 75–100.
Tingay, M., 2015. Initial pore pressures under the Lusi mud volcano, Indonesia. Interpretation 3, SE33–SE49.
Townend, J., Zoback, M.D., 2000. How faulting keeps the crust strong. Geology 28 (5), 399–402.
Van de Weerd, A.A., Ware, P.L.G., 1994. A review of the east Algerian Sahara oil and gas province (triassic, Ghadames and Illizi basins). First Break 12 (7), 363–373.
Wang, H.F., 2000. Theory of Linear Poroelasticity with Applications to Geomechanics and Hydrogeology. Princeton University Press.
Zhang, J., 2011. Pore pressure prediction from well logs: methods, modifications, and new approaches. Earth Sci. Rev. 108 (1–2), 50–63.
Zhang, J., 2013. Borehole stability analysis accounting for anisotropies in drilling to weak bedding planes. Int. J. Rock Mech. Min. Sci. 60, 160–170.
Zoback, M.D., 2007. Reservoir Geomechanics. Stanford University, California.